EDGE ARTICLE

Check for updates

Crystallographic characterization of Y₂C₂ₙ (2n = 82, 88–94): direct Y–Y bonding and cage-dependent cluster evolution†

Changwang Pan,‡[a] Wangqiang Shen,‡[a] Le Yang,‡[b] Lipiao Bao,[a] Zhan Wei,[b] Peng Jin, [ID] *[b] Hongyun Fang,*[a] Yunpeng Xie, [ID] *[a] Takeshi Akasaka[a] and Xing Lu [ID] *[a]

Direct yttrium–yttrium bonding has been a long-sought puzzle in organometallic chemistry to understand the catalytic processes that involve yttrium. Herein, we report the first crystallographic authentication of direct Y–Y bonding inside the hollow cavity of fullerene cages by forming endohedral metallofullerenes (EMFs). Based on an efficient separation/purification process, which involves Lewis-acid treatment and HPLC separation, we have obtained sufficient amounts of a series of Y_2C_{2n} (2n = 82, 88–94) isomers for systematic studies. The unambiguous single-crystal X-ray diffraction (XRD) crystallographic results show that two of them are di-EMFs, namely $Y_2@C_s(6)$-C_{82} and $Y_2@C_{3v}(8)$-C_{82}, in which the long-sought Y–Y single bond between the two divalent yttrium ions is experimentally confirmed for the first time. In contrast, all the other EMFs with relatively large cages are carbide cluster metallofullerenes (CCMFs), namely, $Y_2C_2@C_s(15)$-C_{86}, $Y_2C_2@C_1(26)$-C_{88}, $Y_2C_2@C_2(41)$-C_{90} and $Y_2C_2@C_2(61)$-C_{92}. Consistently, our computational results prove that these experimentally obtained EMFs are all abundant at the high temperatures for fullerene formation (∼1500–3000 K) due to the strong coordination ability of yttrium ions, which enables the formation of either direct Y–Y bonds (for $Y_2@C_s(6)$-C_{82} and $Y_2@C_{3v}(8)$-C_{82}) or the inclusion of a C₂-unit (in $Y_2C_2@C_s(15)$-C_{86}, $Y_2C_2@C_1(26)$-C_{88}, $Y_2C_2@C_2(41)$-C_{90} and $Y_2C_2@C_2(61)$-C_{92}). Our results suggest that metal atoms such as yttrium tend to adopt a low valence state during the arc-discharge process because of the presence of the highly reductive carbon plasma in the chamber, enabling the formation of an Y₂ dimer with direct Y–Y bonding in small cages like C_{82}.

Introduction

The pursuit of novel metal–metal bonds, either supported or unsupported, is of fundamental importance for the in-depth understanding of industrial catalysis, surface chemistry and even bio-inorganic processes.[1] Unsupported bonds are more attractive because ligand bridging may alter the nature of metal–metal bonding.[2] Metal–metal bonds involving elements in the f-block, especially rare-earth metals including scandium and yttrium, have attracted much attention to advance new bonding theory or novel chemical transformations.[3] Most of the studies have focused on the synthesis and characterization of such complexes containing metal–metal bonds between a rare-earth metal and a main group or a transition metal. To the best

of our knowledge, confirmed direct metal–metal bonding between pure rare-earth elements is very rare.[2]

The advent of fullerenes whose hollow cavity can host a variety of metallic elements to form endohedral metal-lofullerenes (EMFs) presents a huge possibility for the investigation of metal–metal interactions by using single crystal X-ray diffraction (XRD) studies.[4–6] Traditional EMFs are those encapsulating one or two metal atoms, which transfer a certain number of electrons to the cage.[7,8] When multiple metal ions are introduced into the cages, a non-metal element is generally required to stabilize the whole cluster to form species such as a metal carbide,[9–11] nitride,[12,13] sulphide,[14] oxide[15–17] and even cyanide.[18,19]

In principle, the positively charged metal ions suffer from strong Coulomb repulsion inside fullerene cages. For example, the estimated repulsion energy between the two La ions in $La_2@C_{80}$ is as high as 10 eV, which is comparable to the dissociation energy of the strongest covalent bonds like the N–N triple bond (9.8 eV).[20] Accordingly, direct (unsupported) metal–metal bonding has not been realized in EMFs until the theoretical analysis of $Y_2@C_{79}N$ revealing a single-electron bond between the two repulsive metal ions.[21] In the following studies, single-electron bonds between two metal ions have also been

aState Key Laboratory of Materials Processing and Die & Mould Technology, School of Materials Science and Engineering, Huazhong University of Science and Technology, 1037 Luoyu Road, Wuhan, 430074 China. E-mail: lux@hust.edu.cn

bSchool of Materials Science and Engineering, Hebei University of Technology, Tianjin, 300130 China. E-mail: china.peng.jin@gmail.com

† Electronic supplementary information (ESI) available. CCDC 1528590, 1528591, 1528691, 1811906, 1812135 and 1812333. For ESI and crystallographic data in CIF or other electronic format see DOI: 10.1039/c9sc00941h

‡ These authors contributed equally to this work.

observed for functionalized or reduced $M_2@C_{80}$ compounds (M = La, Y and Dy).[22–24] These results are explained theoretically by Popov and co-workers by considering metal-localized HOMOs which exhibit pronounced metal–metal bonding character.[20] In addition, theoretical calculations of $Lu_2@C_{76}$ (ref. 25) predicted the presence of a normal metal–metal bond between the two Lu^{2+} ions, and crystallographic evidence for direct Lu–Lu bonding has been reported recently by our group in a series of Lu-containing EMFs, such as $Lu_2@C_{2n}$.[26,27] These results suggest that the confined inner space of fullerene cages can restrict the separation of the repulsive metal ions so as to facilitate the formation of metal–metal bonds, which stimulates us to seek for other unsupported metal–metal bonds between rare earth metals.

Herein, we report the isolation and systematic characterization of a series of di-yttrium EMFs, namely $Y_2@C_s(6)$-C_{82}, $Y_2@C_{3v}(8)$-C_{82}, $Y_2C_2@C_s(15)$-C_{86}, $Y_2C_2@C_1(26)$-C_{88}, $Y_2C_2@C_2(41)$-C_{90} and $Y_2C_2@C_2(61)$-C_{92}. Importantly, this is the first crystallographic identification of di-yttrium EMFs, $Y_2@C_s(6)$-C_{82} and $Y_2@C_{3v}(8)$-C_{82}, featuring unsupported Y–Y bonds. Prior to our work, direct yttrium–yttrium contacts have only been observed in the interstitial compounds Y_4I_5C and $Y_6I_7C_2$ (ref. 28) but never in any organometallic complexes. Interestingly, our results show that the cluster configuration changes from Y_2 to Y_2C_2 as the cage enlarges accompanied by the donation of the valence electrons forming a Y–Y bond with the inserted C_2-unit, and $Y_2C_2@C_{2n}$ ($2n$ = 86–92) are finally formed.

Results and discussion

Soot containing Y_2C_{2n} ($2n$ = 82, 88–94) isomers was synthesized by a direct-current arc discharge method and Y_2C_{2n} isomers were isolated *via* a combinational process involving Lewis-acid treatment and high performance liquid chromatography (HPLC) separation (Fig. S1–S5†). Experimental details are provided in the ESI.† The analytical HPLC chromatograms (Fig. S6†) and the laser-desorption/ionization time-of-flight (LDI-TOF) mass spectra (Fig. S7†) of Y_2C_{2n} ($2n$ = 82, 88–94) reveal their high purity which guarantee the following characterization.

Co-crystals of Y_2C_{2n} ($2n$ = 82, 88–94) with $Ni^{II}(OEP)$ (OEP = 2,3,7,8,12,13,17,18-octaethylporphyrin dianion) were obtained by layering a benzene solution of $Ni^{II}(OEP)$ over the CS_2 solution of each Y_2C_{2n} isomer, and were used to unambiguously determine their molecular structures by single-crystal X-ray diffraction (XRD) crystallography. Details of the crystallographic data are listed in Table S1.† The results unambiguously confirm that two of them are di-EMFs with relatively small cages, namely $Y_2@C_s(6)$-C_{82} and $Y_2@C_{3v}(8)$-C_{82}, whereas the others are all carbide cluster metallofullerenes (CCMFs), *i.e.*, $Y_2C_2@C_s(15)$-C_{86}, $Y_2C_2@C_1(26)$-C_{88}, $Y_2C_2@C_2(41)$-C_{90}, and $Y_2C_2@C_2(61)$-C_{92}, respectively. Although the $C_s(6)$-C_{82}, $C_{3v}(8)$-C_{82} and $C_2(41)$-C_{90} cages have been observed for other EMFs, such as $Lu_2@C_s(6)$-C_{82}, $Lu_2@C_{3v}(8)$-C_{82} and $La_2C_2@C_2(41)$-C_{90},[26,29] the $C_s(15)$-C_{86}, $C_1(26)$-C_{88} and $C_2(61)$-C_{92} cages are unprecedented.

Inside the fullerene cages, the yttrium atoms show some degree of disorder. Details of the disorder are illustrated in Fig. 1 and the occupancy values are summarized in Table S2.† In the two di-EMFs, 8 and 14 yttrium sites were found for the two Y atoms in $C_s(6)$-C_{82} and $C_{3v}(8)$-C_{82}, respectively, indicating a motional behavior of the Y atom to pursue strong yttrium–cage interactions. As for the CCMFs, *i.e.*, $Y_2C_2@C_s(15)$-C_{86}, $Y_2C_2@C_1(26)$-C_{88}, $Y_2C_2@C_2(41)$-C_{90}, and $Y_2C_2@C_2(61)$-C_{92}, the number of the disordered yttrium sites increases along with cage expansion (Fig. 1). In detail, the Y_2C_2 unit displays 4, 4, 8 and 17 sites in $C_s(15)$-C_{86}, $C_1(26)$-C_{88}, $C_2(41)$-C_{90} and $C_2(61)$-C_{92}, respectively. It appears that the motional behavior of the metal atoms inside fullerene cages is an effective way to ensure sufficient metal–cage/metal–C_2 unit interactions.

Moreover, the representative structural data of Y_2C_{2n} ($2n$ = 82, 88–94) isomers, such as the structural parameters of the internal species, and Ni–cage and Y–cage distances, are summarized in Table S3.† In detail, the shortest Y–cage distances are 2.321 Å, 2.357 Å, 2.203 Å, 2.041 Å, 2.010 Å and 2.042 Å for $Y_2@C_s(6)$-C_{82}, $Y_2@C_{3v}(8)$-C_{82}, $Y_2C_2@C_s(15)$-C_{86}, $Y_2C_2@C_1(26)$-C_{88}, $Y_2C_2@C_2(41)$-C_{90} and $Y_2C_2@C_2(61)$-C_{92}, respectively. These values are comparable to those observed for the derivatives of $Y_2C_2@C_s(6)$-C_{82},[30] suggesting strong Y–cage interactions. Moreover, the distances between the Y ions and the internal C_2 units for these CCMFs range from 2.034 Å to
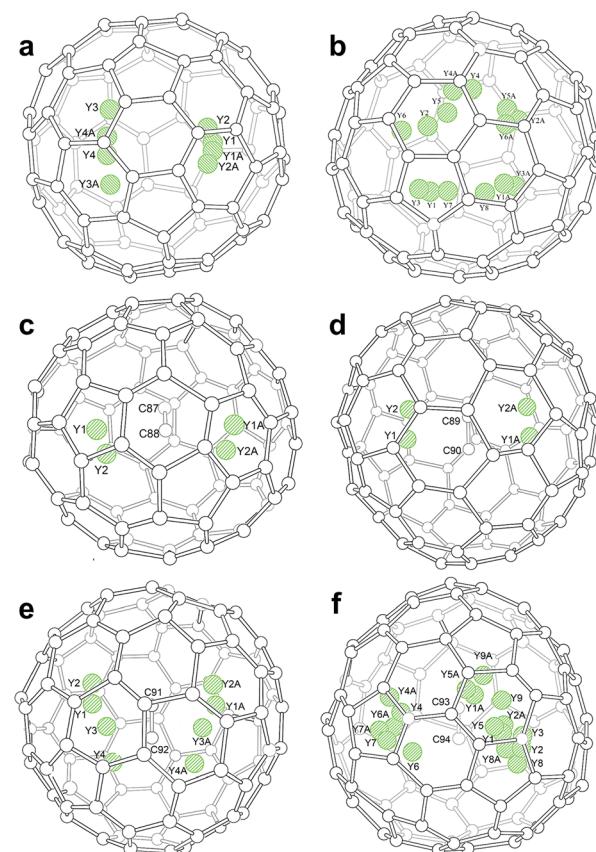
Fig. 1 Perspective drawings showing the internal yttrium sites. (a) 8 in $Y_2@C_s(6)$-C_{82}, (b) 14 in $Y_2@C_{3v}(8)$-C_{82}, (c) 4 in $Y_2C_2@C_s(15)$-C_{86}, (d) 4 in $Y_2C_2@C_1(26)$-C_{88}, (e) 8 in $Y_2C_2@C_2(41)$-C_{90}, and (f) 17 in $Y_2C_2@C_2(61)$-C_{92}.

2.711 Å (Table S3†), which are similar to that observed for $Y_2C_2@C_1(1660)$-C_{108}, representing typical coordination bonds.[31]

Fig. 2 presents the molecular structures of these EMFs showing the major components together with the co-crystallized Ni^{II}(OEP) molecule. The shortest Ni–cage distances range from 2.725 Å to 3.027 Å, suggesting substantial π–π interactions between the fullerene cage and Ni^{II}(OEP). For M$_2$@C$_{2n}$-type EMFs, Popov *et al.* have suggested theoretically that the internal metals may not adopt their highest oxidation states, thus yielding a possibility of covalent metal–metal bonding in such EMFs as $Lu_2@C_{76}$ and $M_2@C_{82}$ (M = Sc, Y, Er, Lu, *etc.*).[20,25,32] Indeed, our concrete crystallographic results reveal that $Lu_2@C_{2n}$ ($2n = 82$–86) are all di-EMFs with a Lu–Lu single bond formed between the two internal lutetium ions.[26] Consistently, formation of the Y–Y bond is also confirmed by our crystallographic results of the two di-EMFs. The Y–Y distances between the major Y sites are 3.635 Å and 3.596 Å for $Y_2@C_{3v}(8)$-C_{82} and $Y_2@C_s(8)$-C_{82}, respectively, which are comparable to the calculated Y–Y single bond length (3.695 Å) for $Y_2@C_{82}$ isomers,[20,32] confirming that each Y atom adopts a low divalent state of +2 and the third valence electron is donated to form the metal–metal bond.

As for the CCMFs, the Y–Y distances between the two major Y sites are 4.121 Å, 4.271 Å, 4.024 Å, and 4.349 Å, for $Y_2C_2@C_s(15)$-C_{86}, $Y_2C_2@C_1(26)$-C_{88}, $Y_2C_2@C_2(41)$-C_{90}, and $Y_2C_2@C_2(61)$-C_{92},

respectively (Table S3†), which are all much longer than the theoretical value of an Y–Y single bond (3.695 Å),[20,32] thus enabling the insertion of a C$_2$-unit to coordinate with the two Y atoms. In addition, the C–C distances of the C$_2$ unit in $Y_2C_2@C_s(15)$-C_{86}, $Y_2C_2@C_1(26)$-C_{88}, $Y_2C_2@C_2(41)$-C_{90}, and $Y_2C_2@C_2(61)$-C_{92} are 1.075 Å, 1.131 Å, 1.052 Å, and 1.046 Å, respectively, indicative of typical C–C triple bonds (Fig. S8 and Table S3†).[33–36]

Fig. 3 shows the visible-near-infrared (Vis-NIR) absorption spectra of the EMFs dissolved in carbon disulfide (CS$_2$) under study, all showing characteristic bands in the range of 400–1400 nm, as summarized in Table S4.† Specifically, the absorption onsets result in a large optical bandgap for $Y_2@C_{3v}(8)$-C_{82} (1.13 eV), small bandgaps for $Y_2C_2@C_s(15)$-C_{86} (0.72 eV) and $Y_2C_2@C_2(41)$-C_{90} (0.86 eV), and moderate bandgaps for $Y_2@C_s(6)$-C_{82} (0.90 eV), $Y_2C_2@C_1(26)$-C_{88} (0.91 eV) and $Y_2C_2@C_2(61)$-C_{92} (0.98 eV).

The two di-EMFs, namely $Y_2@C_{3v}(8)$-C_{82} and $Y_2@C_s(6)$-C_{82}, and the largest CCMF, $Y_2C_2@C_2(61)$-C_{92}, are chosen as representatives for the study of their electrochemical properties by cyclic voltammetry (Fig. S9†), whereas the redox behaviors of the other EMFs under study have not been obtained due to their limited amounts. In general, these three EMFs exhibit one reversible oxidation step and four reversible reduction processes (Fig. S9†). The detailed redox potentials are given in Table 1 along with the values of related EMFs for comparison. It is noteworthy that the first oxidation potentials for the two di-EMFs, *i.e.*, $Y_2@C_s(6)$-C_{82} and $Y_2@C_{3v}(8)$-C_{82}, are identical (-0.16 V), which are much lower than that of $Y_2C_2@C_2(61)$-C_{92} (0.28 V) as well as those of the other di-EMFs reported previously,[22,26,37,38] such as $Sc_2@C_{3v}(8)$-C_{82} (0.05 V), $Lu_2@C_s(6)$-C_{82} (0.34 V) and $La_2@I_h(7)$-C_{80} (0.56 V), revealing their high electron affinity. These results are in good agreement with the speculation by Popov *et al.* and show the metal dependence of the first oxidation potential for di-EMFs with the same cages, which is rationalized through analysis of the energy of M–M bonding molecular orbitals because the electron should be removed from M–M bonding orbitals in the first oxidation process.[32]
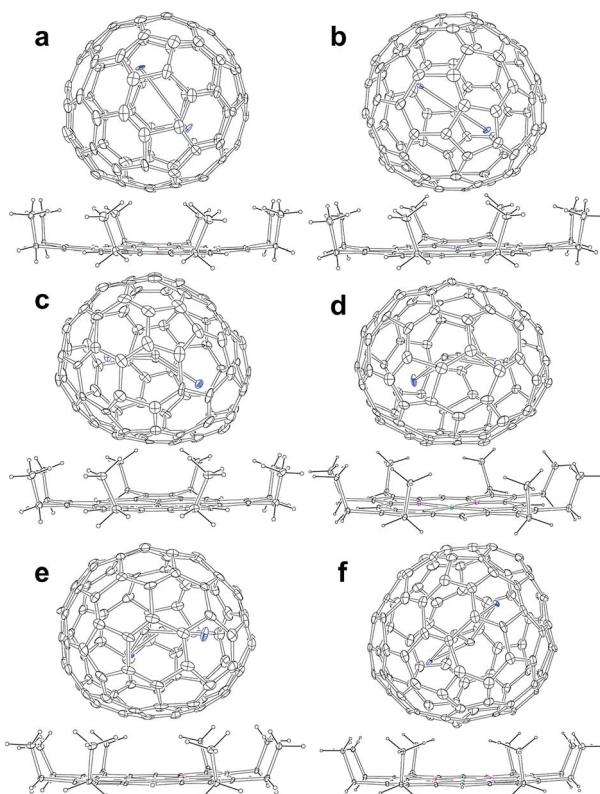
Fig. 2 ORTEP drawings of (a) $Y_2@C_s(6)$-C_{82}, (b) $Y_2@C_{3v}(8)$-C_{82}, (c) $Y_2C_2@C_s(15)$-C_{86}, (d) $Y_2C_2@C_1(26)$-C_{88}, (e) $Y_2C_2@C_2(41)$-C_{90}, and (f) $Y_2C_2@C_2(61)$-C_{92}. Only one cage orientation and the predominant cluster site are shown, while minor sites and solvent molecules are omitted for clarity.
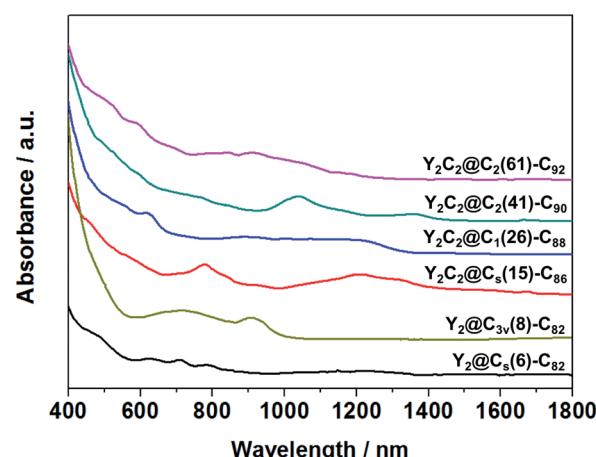
Fig. 3 Vis-NIR absorption spectra of Y_2C_{2n} ($2n = 82$, 88–94) isomers dissolved in CS$_2$.

Table 1 Redox potentials (V *vs.* Fc/Fc$^+$)^a of Y$_2$@C_{3v}(8)-C$_{82}$, Y$_2$@C_s(6)-C$_{82}$ and Y$_2$C$_2$@C_2(61)-C$_{92}$ along with those of related EMFs

| EMFs	$^{ox}E_1$	$^{red}E_1$	$^{red}E_2$	$^{red}E_3$	$^{red}E_3$	E_{gap}^{b}	Ref.
Y$_2$@C_{3v}(8)-C$_{82}$	−0.16	−1.23	−1.61	−2.18	−2.46	1.07	This work
Sc$_2$@C_{3v}(8)-C$_{82}$	0.02	−1.16	−1.53	−1.73	−2.02	1.18	32
Er$_2$@C_{3v}(8)-C$_{82}$	0.13	−1.14	−1.41	−1.83	—	1.27	32
Lu$_2$@C_{3v}(8)-C$_{82}$	0.50	−1.16	−1.46	−1.77	—	1.66	32
Y$_2$@C_s(6)-C$_{82}$	−0.16	−1.06	−1.39	−1.85	−2.15	0.90	This work
Er$_2$@C_s(6)-C$_{82}$	0.02	−1.01	−1.31	—	—	1.03	32
Lu$_2$@C_s(6)-C$_{82}$	0.34	−1.02	−1.35	−1.77	—	1.36	26
Y$_2$C$_2$@C_2(61)-C$_{92}$	0.28	−1.00	−1.49	−1.73	−1.98	1.28	This work

^{a} Half-cell potentials are given unless otherwise stated. ^{b} $E_{gap} = (^{ox}E_1 - {}^{red}E_1)$.

Hence the lowest first oxidation potential of Y$_2$@C$_{82}$ (*e.g.*, C_{3v}(8)- or C_s(6)-C$_{82}$) among M$_2$@C$_{82}$ (M = Sc, Y, Lu and Er) is probably ascribed to the high energy of the Y–Y bonding orbital.[20] In addition, the redox potentials of Y$_2$@C_{3v}(8)-C$_{82}$ are cathodically shifted as compared to the corresponding values of M$_2$@C_{3v}(8)-C$_{82}$ (M = Sc, Er and Lu),[32] indicating that the electrochemical properties of EMFs can be readily manipulated by adjusting the encapsulated species inside the cages.

Density functional theory (DFT) calculations at the M06-2X/6-31G*∼SDD level were conducted to rationalize the formation of these stable Y$_2$C$_{2n}$ (2n = 82, 88–94) isomers. Fig. S10† depicts their optimized geometries, which agree well with the X-ray structures. For the two di-EMFs, the optimized Y–Y distances are 3.60 Å and 3.54 Å for Y$_2$@C_s(6)-C$_{82}$ and Y$_2$@C_{3v}(8)-C$_{82}$, respectively, which are consistent with our crystallographic results, clearly indicating a direct Y–Y bond between the two yttrium ions. Moreover, it was proposed that both the C_s(6)-C$_{82}$ and C_{3v}(8)-C$_{82}$ cages have a low-lying LUMO and LUMO+1, but a high-lying LUMO+2, whose energies are higher than that of the Y–Y bonding MO.[20] Therefore, the two Y atoms ([Kr]4d^{1}5s^2) tend to adopt the divalent state with the remaining two electrons pairing to generate an Y–Y single bond. Indeed, our calculations for Y$_2$, C_s(6)-C$_{82}$, C_{3v}(8)-C$_{82}$, Y$_2$@C_s(6)-C$_{82}$ and Y$_2$@C_{3v}(8)-C$_{82}$ confirm that there are large energy gaps between the LUMO+2 of the two hollow cages and the HOMOs of the Y$_2$ dimer, implying unfavorable electron transfer from the latter to the former (Fig. S11†). Further natural bond orbital (NBO) analysis demonstrates that the two Y atoms in the two Y$_2$@C$_{82}$ isomers form an Y–Y single bond with an electron occupancy of 1.97 e, which is supported by the calculated Wiberg bond orders (WBOs) for Y$_2$@C_s(6)-C$_{82}$ and Y$_2$@C_{3v}(8)-C$_{82}$ ranging from 1.11 to 1.12 (Table S5†). The Y–Y bonds have spd-hybrid character with the Y-5s orbitals contributing the most to the metal bonding MOs, and each Y atom donates one 4d electron and one 5s electron to the cage.

As for the CCMFs, however, the calculated Y–Y distances in Y$_2$C$_2$@C_s(15)-C$_{86}$, Y$_2$C$_2$@C_1(26)-C$_{88}$, Y$_2$C$_2$@C_2(41)-C$_{90}$, and Y$_2$C$_2$@C_2(61)-C$_{92}$ are as long as 4.53 Å, 4.25 Å, 4.40 Å and 4.56 Å, respectively, which are consistent with the X-ray diffraction values, indicating the absence of direct Y–Y bonding. Consistently, the calculated WBO values for these CCMFs range from 0.29 to 0.41 (Table S5†), revealing clearly that the valence electrons forming the Y–Y bond in di-EMFs are donated to the C$_2$-unit to form the CCMFs.

Further computational studies were done on different low-lying Y$_2$C$_{2n}$ (2n = 82, 88–94) isomers in either the Y$_2$@C$_{2n}$ or Y$_2$C$_2$@C$_{2n−2}$ form to rationalize the existence of the experimentally obtained Y$_2$C$_{2n}$ isomers. Fig. S12† to S16 show their optimized structures and relative energies as well as HOMO–LUMO gap energies. Since fullerenes and EMFs are formed at very high temperatures (1500–3000 K) under arc discharge conditions,[39] we have also analyzed the relative stability of the most favorable EMFs in terms of their relative Gibbs free energies.[40] As clearly shown in Fig. S12†, Y$_2$@C_s(6)-C$_{82}$ and Y$_2$@C_{3v}(8)-C$_{82}$ are the lowest-energy ones among all the considered isomers, and Fig. 4a clearly shows that they are the most abundant isomers in the temperature range for EMF formation. In comparison, when the number of carbon atoms increases from C$_{88}$ to C$_{90}$, our calculations reveal that the experimentally obtained CCMF isomers, Y$_2$C$_2$@C_s(15)-C$_{86}$ and Y$_2$C$_2$@C_1(26)-C$_{88}$, are more than 8.2 kcal mol^{-1} higher in energy
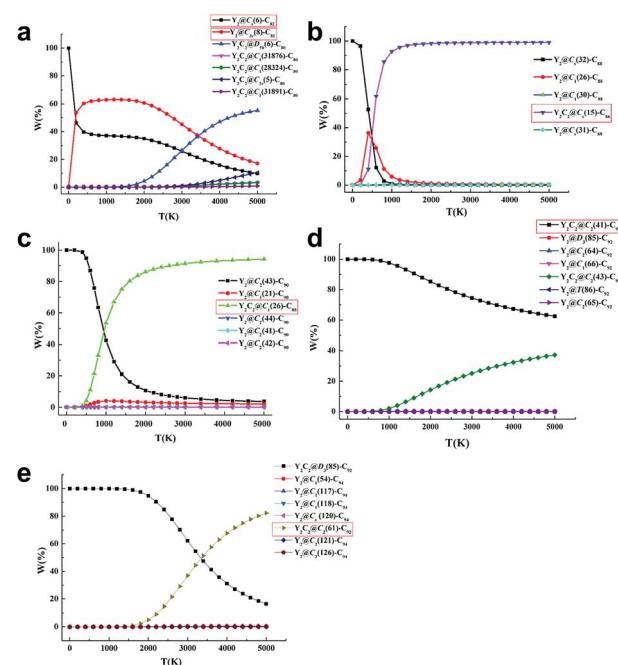
Fig. 4 Computed molar fraction as a function of temperature for the low-lying isomers of (a) Y$_2$C$_{82}$, (b) Y$_2$C$_{88}$, (c) Y$_2$C$_{90}$, (d) Y$_2$C$_{92}$, and (e) Y$_2$C$_{94}$. The isomers marked with red boxes are experimentally obtained.

than the corresponding lowest-lying di-EMFs isomers (Fig. S13 and S14†). However, when the Gibbs energy is taken into account, they become the most abundant isomers above 1500 K, with the molar fractions of the corresponding di-EMFs being almost negligible (Fig. 4b and c).

As for Y_2C_{92-94}, $Y_2C_2@C_2(41)$-C_{90}, $Y_2C_2@C_2(61)$-C_{92} and their corresponding di-EMF isomers are mixed in terms of their potential energy, and the most stable Y_2C_{92} and Y_2C_{94} are both CCMFs, namely, $Y_2C_2@C_2(41)$-C_{90} and $Y_2C_2@D_3(85)$-C_{92}, respectively (Fig. S15 and S16†). From Fig. 4d, we can see that $Y_2C_2@C_2(41)$-C_{90} is the dominant species in the whole range of temperatures up to 5000 K. Moreover, as for Y_2C_{94}, although $Y_2C_2@D_3(85)$-C_{92} is the dominant species at low temperatures, the concentration of the experimentally obtained $Y_2C_2@C_2(61)$-C_{92} rapidly increases when the temperature rises, finally surpassing that of $Y_2C_2@D_3(85)$-C_{92} after 3400 K (Fig. 4e).

Overall, our experimental and theoretical results have unambiguously confirmed that the Y_2 dimer chose to form a Y–Y single bond in relatively small cages like C_{82}, but the cluster configuration changes from Y_2 to Y_2C_2 when the cage expands, thus forming the CCMFs in large cages C_{86-92}. It is inferred that larger metals such as erbium and lanthanum may prefer a larger cage to form the corresponding CCMFs. For example, Stevenson *et al.* reported the isolation and crystallographic characterization of an erbium-based CCMF with a giant C_{92} cage, namely $Er_2C_2@D_3(85)$-C_{92}.[41] Moreover, our group found that the even larger La^{3+} ions tend to form CCMFs with some giant cages such as C_{90-104}.[29,35,36] In addition, the cluster configuration is another critical factor that may affect the cage size. For instance, a linear Y_2C_2 cluster can be encapsulated into the giant C_{108} cage to template the formation of $Y_2C_2@C_1(1660)$-C_{108}.[31] There is still a long way to finally clarify the mysteries in the metal–metal interactions in EMFs and new theories of coordination chemistry are expected.

Conclusions

A series of di-yttrium EMFs Y_2C_{2n} ($2n$ = 82, 88–94) have been successfully isolated and fully characterized by mass spectrometry, UV-vis-NIR and single-crystal X-ray crystallography. The crystallographic results unambiguously confirm that two of them are di-EMFs, namely $Y_2@C_s(6)$-C_{82} and $Y_2@C_{3v}(8)$-C_{82}, whereas the others are all CCMFs, *i.e.*, $Y_2C_2@C_s(15)$-C_{86}, $Y_2C_2@C_1(26)$-C_{88}, $Y_2C_2@C_2(41)$-C_{90}, and $Y_2C_2@C_2(61)$-C_{92}, respectively. It is noteworthy that our experimental and theoretical studies clearly reveal that the Y_2 dimer preferentially forms a Y–Y single bond in the di-EMFs with small cages, and further cage expansion alters its configuration to Y_2C_2 because the valence electrons forming the Y–Y bond are donated to the inserted C_2-unit, thus resulting in the formation of the corresponding CCMFs in larger cages. In addition, our computational results demonstrate that the high thermodynamic stability of all these EMFs originates from a four-electron transfer and the bonding nature between the internal metallic species and cages. Accordingly, this work has confirmed for the first time the existence of the Y–Y bond inside fullerene cages and the transformation from di-EMFs to CCMFs along with the cage expansion, presenting an in-depth understanding and new sights into the metal–metal/metal–carbon interactions in such rarely explored metal–carbon hybrid molecules.

Experimental section

Synthesis of Y_2C_{2n} ($2n$ = 82, 88–94) isomers

Soot containing yttrium-EMFs was synthesized using a direct-current arc discharge method. Briefly, a core-drilled graphite rod filled with graphite/Y_2O_3 (molar ratio: Y/C = 1 : 50) was burned under a 225 Torr helium atmosphere with a power of 100 A × 20 V. The soot was then extracted with CS_2. After removal of CS_2, the residue was dissolved in toluene and the solution was subjected to high performance liquid chromatography (HPLC) for the subsequent separation. After a combinational process involving Lewis-acid treatment and multi-stage HPLC separation, six pure isomers of yttrium-EMFs are finally obtained. Experimental details are described in the ESI.†

Co-crystallization and crystallographic solutions of Y_2C_{2n} ($2n$ = 82, 88–94) cocrystals

Crystalline blocks of $Y_2C_2@C_{2n}\cdot Ni(OEP)$ were obtained by layering a benzene solution of Ni(OEP) over a CS_2 solution of the corresponding metallofullerene at room temperature for two weeks. Single-crystal XRD measurements of $Y_2C_2@C_1(26)$-C_{88} and $Y_2@C_{3v}(8)$-C_{82} were performed at 173 K on a Bruker D8 QUEST machine equipped with a CMOS camera (Bruker AXS Inc., Germany), and X-ray data of $Y_2@C_s(6)$-C_{82} were obtained at 100 K at the BL17U station of the Shanghai Synchrotron Radiation Facility. Crystallographic characterization of the other three EMFs, *i.e.*, $Y_2C_2@C_s(15)$-C_{86}, $Y_2C_2@C_2(41)$-C_{90}, and $Y_2C_2@C_2(61)$-C_{92}, was performed at 100 K at the BL17B station of the Shanghai Synchrotron Radiation Facility. The multi-scan method was used for absorption corrections. The structures were solved by the direct method and were refined with SHELXL-2014/7.[42] Co-crystals of $Y_2@C_{3v}(8)$-$C_{82}\cdot Ni^{II}(OEP)$ and $Y_2C_2@C_2(61)$-$C_{92}\cdot Ni^{II}(OEP)$ contain a severely disordered lattice of C_6H_6 and CS_2 molecules that could not be modeled properly. Therefore, the SQUEEZE program, a part of the PLATON package of crystallographic software,[43,44] was used to calculate the solvent disorder area and remove its contribution from the intensity data. CCDC-1811906 ($Y_2@C_s(6)$-C_{82}), CCDC-1812333 ($Y_2@C_{3v}(8)$-C_{82}), CCDC-1528591 ($Y_2C_2@C_s(15)$-C_{86}), CCDC-1528590 ($Y_2C_2@C_1(26)$-C_{88}), CCDC-1528691 ($Y_2C_2@C_2(41)$-C_{90}), and CCDC-1812135 ($Y_2C_2@C_2(61)$-C_{92}) contain the supplementary crystallographic data for this paper.†

Computational details

Density functional theory calculations were carried out by using the M06-2X[45] functional in conjunction with the 6-31G* basis set for C[46,47] and SDD basis set and the corresponding effective core potential for Y[48] (denoted as 6-31G*~SDD), as implemented in the Gaussian 09 software package.[49] More details are given in the ESI.†

Conflicts of interest

There are no conflicts to declare.

Acknowledgements

Notes and references

1 M. S. Hill, P. B. Hitchcock and R. Pongtavornpinyo, *Science*, 2006, **311**, 1904–1907.
2 M. V. Butovskii and R. Kempe, *New J. Chem.*, 2015, **39**, 7544–7558.
3 S. T. Liddle and D. P. Mills, *Dalton Trans.*, 2009, 5592–5605.
4 L. Bao, P. Peng and X. Lu, *Acc. Chem. Res.*, 2018, **51**, 810–815.
5 A. A. Popov, S. Yang and L. Dunsch, *Chem. Rev.*, 2013, **113**, 5989–6113.
6 X. Lu, L. Feng, T. Akasaka and S. Nagase, *Chem. Soc. Rev.*, 2012, **41**, 7723.
7 X. Zhang, Y. Wang, R. Morales-Martínez, J. Zhong, C. de Graaf, A. Rodríguez-Fortea, J. M. Poblet, L. Echegoyen, L. Feng and N. Chen, *J. Am. Chem. Soc.*, 2018, **140**, 3907–3915.
8 W. Cai, R. Morales-Martínez, X. Zhang, D. Najera, E. L. Romero, A. Metta-Magaña, A. Rodríguez-Fortea, S. Fortier, N. Chen, J. M. Poblet and L. Echegoyen, *Chem. Sci.*, 2017, **8**, 5282–5290.
9 T.-S. Wang, N. Chen, J.-F. Xiang, B. Li, J.-Y. Wu, W. Xu, L. Jiang, K. Tan, C.-Y. Shu, X. Lu and C.-R. Wang, *J. Am. Chem. Soc.*, 2009, **131**, 16646–16647.
10 H. Fang, H. Cong, M. Suzuki, L. Bao, B. Yu, Y. Xie, N. Mizorogi, M. M. Olmstead, A. L. Balch, S. Nagase, T. Akasaka and X. Lu, *J. Am. Chem. Soc.*, 2014, **136**, 10534–10540.
11 C.-H. Chen, K. B. Ghiassi, M. R. Cerón, M. A. Guerrero-Ayala, L. Echegoyen, M. M. Olmstead and A. L. Balch, *J. Am. Chem. Soc.*, 2015, **137**, 10116–10119.
12 T. Cai, L. Xu, M. R. Anderson, Z. Ge, T. Zuo, X. Wang, M. M. Olmstead, A. L. Balch, H. W. Gibson and H. C. Dorn, *J. Am. Chem. Soc.*, 2006, **128**, 8581–8589.
13 S. Stevenson, H. M. Lee, M. M. Olmstead, C. Kozikowski, P. Stevenson and A. L. Balch, *Chem.–Eur. J.*, 2002, **8**, 4528–4535.
14 N. Chen, M. N. Chaur, C. Moore, J. R. Pinzón, R. Valencia, A. Rodríguez-Fortea, J. M. Poblet and L. Echegoyen, *Chem. Commun.*, 2010, **46**, 4818–4820.
15 S. Stevenson, M. A. Mackey, M. A. Stuart, J. P. Phillips, M. L. Easterling, C. J. Chancellor, M. M. Olmstead and A. L. Balch, *J. Am. Chem. Soc.*, 2008, **130**, 11844–11845.
16 B. Q. Mercado, M. M. Olmstead, C. M. Beavers, M. L. Easterling, S. Stevenson, M. A. Mackey, C. E. Coumbe, J. D. Phillips, J. Paige Phillips, J. M. Poblet and A. L. Balch, *Chem. Commun.*, 2010, **46**, 279–281.
17 Q. Tang, L. Abella, Y. Hao, X. Li, Y. Wan, A. Rodríguez-Fortea, J. M. Poblet, L. Feng and N. Chen, *Inorg. Chem.*, 2015, **54**, 9845–9852.
18 T.-S. Wang, L. Feng, J.-Y. Wu, W. Xu, J.-F. Xiang, K. Tan, Y.-H. Ma, J.-P. Zheng, L. Jiang, X. Lu, C.-Y. Shu and C.-R. Wang, *J. Am. Chem. Soc.*, 2010, **132**, 16362–16364.
19 F. Liu, C.-L. Gao, Q. Deng, X. Zhu, A. Kostanyan, R. Westerström, S. Wang, Y.-Z. Tan, J. Tao, S.-Y. Xie, A. A. Popov, T. Greber and S. Yang, *J. Am. Chem. Soc.*, 2016, **138**, 14764–14771.
20 A. A. Popov, S. M. Avdoshenko, A. M. Pendás and L. Dunsch, *Chem. Commun.*, 2012, **48**, 8031.
21 T. Zuo, L. Xu, C. M. Beavers, M. M. Olmstead, W. Fu, T. D. Crawford, A. L. Balch and H. C. Dorn, *J. Am. Chem. Soc.*, 2008, **130**, 12992–12997.
22 L. Bao, M. Chen, C. Pan, T. Yamaguchi, T. Kato, M. M. Olmstead, A. L. Balch, T. Akasaka and X. Lu, *Angew. Chem., Int. Ed.*, 2016, **55**, 4242–4246.
23 M. Yamada, H. Kurihara, M. Suzuki, M. Saito, Z. Slanina, F. Uhlik, T. Aizawa, T. Kato, M. M. Olmstead, A. L. Balch, Y. Maeda, S. Nagase, X. Lu and T. Akasaka, *J. Am. Chem. Soc.*, 2015, **137**, 232–238.
24 F. Liu, D. S. Krylov, L. Spree, S. M. Avdoshenko, N. A. Samoylova, M. Rosenkranz, A. Kostanyan, T. Greber, A. U. B. Wolter, B. Büchner and A. A. Popov, *Nat. Commun.*, 2017, **8**, 16098.
25 T. Yang, X. Zhao and E. Osawa, *Chem.–Eur. J.*, 2011, **17**, 10230–10234.
26 W. Shen, L. Bao, Y. Wu, C. Pan, S. Zhao, H. Fang, Y. Xie, P. Jin, P. Peng, F.-F. Li and X. Lu, *J. Am. Chem. Soc.*, 2017, **139**, 9979–9984.
27 W. Shen, L. Bao, S. Hu, L. Yang, P. Jin, Y. Xie, T. Akasaka and X. Lu, *Chem. Sci.*, 2019, **10**, 829–836.
28 S. M. Kauzlarich, T. Hughbanks, J. D. Corbett, P. Klavins and R. N. Shelton, *Inorg. Chem.*, 1988, **27**, 1791–1797.
29 S. Zhao, P. Zhao, W. Cai, L. Bao, M. Chen, Y. Xie, X. Zhao and X. Lu, *J. Am. Chem. Soc.*, 2017, **139**, 4724–4728.
30 F. Jin, N. B. Tamm, S. I. Troyanov and S. Yang, *J. Am. Chem. Soc.*, 2018, **140**, 3496–3499.
31 C. Pan, L. Bao, X. Yu, H. Fang, Y. Xie, T. Akasaka and X. Lu, *ACS Nano*, 2018, **12**, 2065–2069.
32 N. A. Samoylova, S. M. Avdoshenko, D. S. Krylov, H. R. Thompson, A. C. Kirkhorn, M. Rosenkranz, S. Schiemenz, F. Ziegs, A. U. B. Wolter, S. Yang, S. Stevenson and A. A. Popov, *Nanoscale*, 2017, **23**, 7977–7990.
33 C.-H. Chen, L. Abella, M. R. Cerón, M. A. Guerrero-Ayala, A. Rodríguez-Fortea, M. M. Olmstead, X. B. Powers, A. L. Balch, J. M. Poblet and L. Echegoyen, *J. Am. Chem. Soc.*, 2016, **138**, 13030–13037.
34 H. Yang, C. Lu, Z. Liu, H. Jin, Y. Che, M. M. Olmstead and A. L. Balch, *J. Am. Chem. Soc.*, 2008, **130**, 17296–17300.

35 W. Cai, F.-F. Li, L. Bao, Y. Xie and X. Lu, *J. Am. Chem. Soc.*, 2016, **138**, 6670–6675.

36 W. Cai, L. Bao, S. Zhao, Y. Xie, T. Akasaka and X. Lu, *J. Am. Chem. Soc.*, 2015, **137**, 10292–10296.

37 M. Yamada, M. Minowa, S. Sato, Z. Slanina, T. Tsuchiya, Y. Maeda, S. Nagase and T. Akasaka, *J. Am. Chem. Soc.*, 2011, **133**, 3796–3799.

38 H. Kurihara, X. Lu, Y. Iiduka, N. Mizorogi, Z. Slanina, T. Tsuchiya, S. Nagase and T. Akasaka, *Chem. Commun.*, 2012, **48**, 1290–1292.

39 W. Krätschmer, L. D. Lamb, K. Fostiropoulos and D. R. Huffman, *Nature*, 1990, **347**, 354–358.

40 Z. Slanina, S.-L. Lee, F. Uhlík, L. Adamowicz and S. Nagase, *Theor. Chem. Acc.*, 2007, **117**, 315–322.

41 A. L. Balch, M. M. Olmstead, X. Powers, C. M. Davison, S. Stevenson and K. R. Tepper, *Chem.–Eur. J.*, 2018, **24**, 13479–13484.

42 G. M. Sheldrick, *Acta Crystallogr., Sect. A: Found. Crystallogr.*, 2008, **64**, 112–122.

43 A. L. Spek, *J. Appl. Crystallogr.*, 2003, **36**, 7–13.

44 P. van der Sluis and A. L. Spek, *Acta Crystallogr., Sect. A: Found. Crystallogr.*, 1990, **46**, 194–201.

45 Y. Zhao and D. G. Truhlar, *Theor. Chem. Acc.*, 2008, **120**, 215–241.

46 G. A. Petersson and M. A. Al-Laham, *J. Chem. Phys.*, 1991, **94**, 6081–6090.

47 G. A. Petersson, A. Bennett, T. G. Tensfeldt, M. A. Al-Laham, W. A. Shirley and J. Mantzaris, *J. Chem. Phys.*, 1988, **89**, 2193–2218.

48 X. Cao and M. Dolg, *J. Mol. Struct.: THEOCHEM*, 2002, **581**, 139–147.

49 M. J. Frisch, G. W. Trucks, H. B. Schlegel, G. E. Scuseria, M. A. Robb, J. R. Cheeseman, G. Scalmani, V. Barone, B. Mennucci and G. A. Petersson, *et al.*, *Gaussian 09*, Gaussian, Inc., Wallingford, CT, USA, 2009.